Extended convolution model for computing the far-field directivity of an amplitude-modulated parametric loudspeaker

Chuang Shi
University of Electronic Science and Technology of China, Chengdu, China
E-mail: shichuang@uestc.edu.cn

Yue Wang
University of Electronic Science and Technology of China, Chengdu, China
E-mail: wangyue2020@std.uestc.edu.cn

Han Xiao
University of Electronic Science and Technology of China, Chengdu, China
E-mail: han.xiao@std.uestc.edu.cn

Huiyong Li
University of Electronic Science and Technology of China, Chengdu, China
E-mail: hyli@uestc.edu.cn

December 2021

Abstract. The convolution model of the parametric loudspeaker describes the far-field directivity of the difference-frequency wave by the product directivity of two ultrasonic primary frequencies convolved with Westervelt's directivity. This can be extended to the case when the primary wave is amplitude-modulated thus resulting in the harmonic distortion of the self-demodulated wave. This paper proposes the extended convolution model with Westervelt's directivity and Berktay's directivity respectively. The angle-dependent harmonic distortion of the parametric loudspeaker is thereafter investigated, which is a topic not often mentioned in previous literature but is of significance in practice. The measurement, numerical simulation and model results are compared for the case when the double sideband (DSB) modulation is adopted and the frequency response of the ultrasonic emitter is a known factor. The comparison validates that the extended convolution model provides accurate predictions that are consistent with the measurement results and the extended convolution model is a simpler way to compute the far-field directivity of an amplitude-modulated parametric loudspeaker as compared to the numerical simulation.

Keywords: Parametric loudspeaker, extended convolution model, Westervelt's

directivity, Berktay's directivity, amplitude modulation

Submitted to: *J. Phys. D: Appl. Phys.*

1. Introduction

Due to the parametric array effect, when two ultrasonic primary frequencies are transmitted at the same angle, the virtual sources of the difference frequency are created and form an end-fire array [1, 2]. If the primary wave is excited by a modulated ultrasonic carrier, the self-demodulated wave is generated in a similar manner, which can be interpreted as the difference frequency between the sideband frequency and the carrier frequency [3]. The self-demodulated wave possesses a narrow directivity, which is similar to the directivity of the ultrasonic carrier. Therefore, the parametric loudspeaker modulates an audio input on the ultrasonic carrier, transmits the modulated ultrasound carrier through a small-sized ultrasonic emitter, and is finally able to present an audio beam in air [4]. The Berktay's far-field solution describes the self-demodulation process concisely by a square function and a high-pass filter. It has been well understood that the square function introduces harmonic distortion, while the high-pass filter affects the frequency response of the parametric loudspeaker [5].

The state-of-the-art approaches to reduce the harmonic distortion of the parametric loudspeaker include a selection of modulation and preprocessing methods. The amplitude modulation, more specifically called the double sideband (DSB) modulation, is shown in figure 1(a). It was the first modulation method studied for the parametric loudspeaker [4]. Due to the two sidebands, the DSB modulation suffers from the second harmonic distortion, of which the level is proportional to the modulation index. Adding in a quadrature term, the single sideband (SSB) modulation was proposed as a variant of the DSB modulation [6]. Block diagrams of the lower and upper SSB modulations are shown in figure 1(b) and figure 1(c), respectively. When the audio input is a sinusoid signal, the SSB modulation outputs two ultrasonic primary frequencies that ideally eliminate the harmonic distortion resultant from the second-order nonlinearity of air.

Alternatively, the square root method was proposed as a preprocessing method for the DSB modulation [7]. The square root is an inverse operator to the square function in the Berktay's far-field solution. Moreover, equalization of the ultrasonic emitter before the square root method is expected to improve the performance in practice [8]. A post equalization is usually carried out by the double integral to offset the high-pass filter in the Berktay's far-field solution [9]. The automatic gain control is another type of preprocessing method that changes the dynamic range of the modulated ultrasonic carrier to reduce the effective modulation index and subsequently result in a lower harmonic distortion level of a variety of modulation methods [10]. Recently, the Volterra filter based linearization technique has demonstrated to be the most versatile and effective preprocessing method if the computational complexity does not affect its implementation [11].

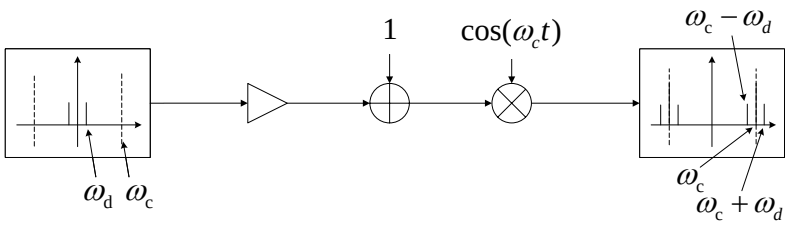

(a) Double sideband modulation

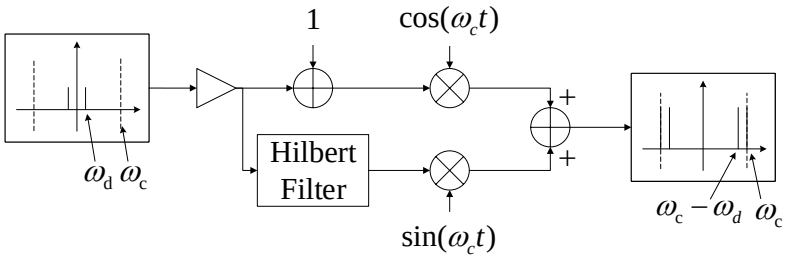

(b) Lower single sideband modulation

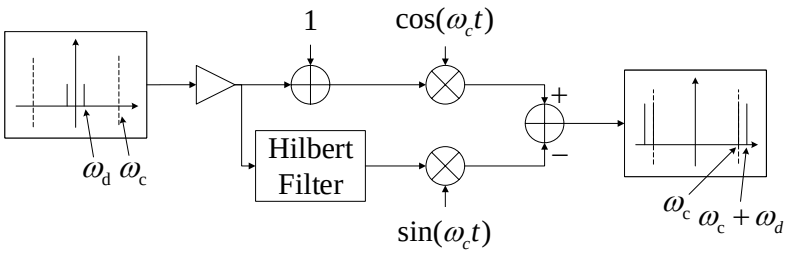

(c) Upper single sideband modulation

Figure 1. Block diagrams of the (a) DSB, (b) lower and (c) upper SSB modulations.

Once the harmonic distortion problem can be resolved, the parametric loudspeaker will become a very convenient directional sound source that can be readily applied in a wide range of sound field control applications. Differing from the conventional loudspeaker array, the parametric loudspeaker is a small-sized stand-alone unit that requires no additional directivity control. Many attempts have been reported regarding applications of the parametric loudspeaker in active noise control [12], audio projection [13], human-machine interface [14], and increasingly in contemporary art projects [15, 16]. In the above mentioned instances, the emphasis has been given to the narrow directivity and small size of the parametric loudspeaker, but the sound quality remains unaddressed.

Applications of the parametric loudspeaker have necessitated a directivity model of the self-demodulated wave to incorporate with modulation methods that can reduce the harmonic distortion. Besides the axial performance of the parametric loudspeaker,

the beam patterns of the difference-frequency wave and its harmonics are investigated. Listeners found themselves very likely to stand on an off-axis angle of the audio beam system, due to the narrow directivity of the parametric loudspeaker [17]. It was also noted in [18] that using the parametric loudspeaker at an off-axis angle could reduce the risk of ultrasound exposure.

The product directivity principle is the basis of many models that were used for computing the far-field directivity of the difference-frequency wave. Based on the product directivity principle, the directivity of the difference-frequency wave is simply estimated by the product of the beam patterns of two ultrasonic primary frequencies, which becomes unreasonably narrower than the directivity of the primary wave. However, the product directivity principle was adopted in early designs of the steerable parametric loudspeaker, whereby beam patterns of the two ultrasonic primary frequencies were steered to the target angle of the difference-frequency wave [19]. After that, the product directivity principle was modified using ad hoc methods, such as introducing the equivalent Gaussian source array and carrying out the spline interpolation between local peaks of the model result, until the convolution model was formulated based on Westervelt's derivation [20].

The convolution model describes the far-field directivity of the difference-frequency wave by the product directivity of two ultrasonic primary frequencies convolved with the so-called Westervelt's directivity. It provides an accurate and concise directivity model for the parametric loudspeaker. The convolution model has been successfully adopted in the reproduction of personal sound in shared environments [21]. In the design of an omnidirectional parametric loudspeaker [22], the convolutional model was adapted to the case of a curved ultrasonic emitter [23]. On the other hand, the convolution model may not capture the complex near field nonlinear interactions between the ultrasonic waves [24]. Therefore, a cylindrical expansion for the ultrasound was introduced when the radiating surface of the ultrasonic emitter was modeled as a baffled phased ultrasonic source [25]. The resultant directivity model improves the accuracy of the convolution model but increases the computation complexity greatly.

So far, the convolution model is only applicable to the parametric loudspeaker using the SSB modulation. In order to compute the directivity of the parametric loudspeaker using the DSB and other amplitude modulations, this paper proposes an extended convolution model based on the spectral analysis of the self-demodulated wave, resulting in the extended convolution model with Westervelt's directivity. Moreover, the Berktay's far-field solution is also examined and extended, resulting in the extended convolution model with Berktay's directivity. Using both numerical simulations and experimental measurements, the proposed extended convolution models are validated.

2. Theory

Assumptions made in Westervelt's original derivation are invoked [2]. Two ultrasonic primary frequencies are transmitted in extremely narrow and perfectly collimated

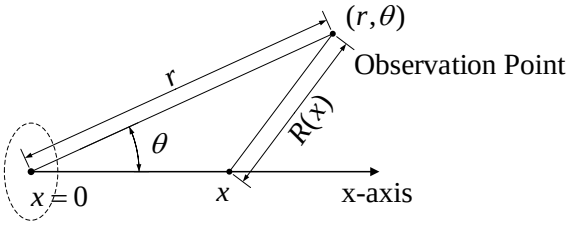

Figure 2. Geometry of the theoretical derivation.

beams, so that the volume distribution of virtual sources of the secondary wave is represented adequately by a line distribution along the propagation direction of the primary wave. The cross-section area is assumed to be a unit. There is no attenuation of the difference-frequency wave and the nonlinear attenuation of the primary sound field is negligible. Hence, the pressure level of the primary sound field at a distance x and time t is considered in the form of

$$p_i(x,t) = \sum_{n=1}^{2} P_n e^{-\alpha_n x} \cos(\omega_n t - k_n x), \tag{1}$$

where P_n, α_n, ω_n, and k_n are the amplitude, attenuation rate, angular frequency, and wavenumber of the n-th primary frequency, respectively.

Based on Lighthill's equation, Westervelt has derived the source strength density of the secondary waves as

$$q(x,t) = \frac{\beta}{\rho_0^2 c_0^4} \frac{\partial}{\partial t} p_i^2(x,t), \tag{2}$$

where β is the nonlinear coefficient; ρ_0 is the density of the medium; and c_0 is the sound speed in the medium at infinitesimal amplitude. Substitute (1) into (2) and discard the second harmonic and sum-frequency terms. The difference-frequency source strength density of the secondary wave is thereafter extracted as

$$q_d(x,t) = \frac{\beta}{\rho_0^2 c_0^4} \omega_d P_1 P_2 e^{-\alpha_{(1,2)} x} \sin(k_d x - \omega_d t), \tag{3}$$

where $\alpha_{(1,2)}$ is the sum of α_1 and α_2; k_d and ω_d are the wavenumber and angular frequency of the difference-frequency wave, respectively.

Under the far-field and absorption-limited source conditions, the pressure level of the difference-frequency wave is simplified into a linear integral, which is given by

$$p_d(r,\theta,t) = \frac{\rho_0}{4\pi} \int_0^{+\infty} \frac{1}{R(x)} \frac{\partial}{\partial t} q_d \left(x, t - \frac{R(x)}{c_0} \right) dx, \tag{4}$$

where r is the distance from an observation point to the origin; θ is the off-axis angle of the observation point with respect to the x-axis; and $R(x)$ is the distance from the observation point to a virtual source located at x. The geometry is shown in figure 2. $R(x)$ can be approximated by r in the denominator and by $r - x + x\ tan^2(\theta)/2$ in the

retarded time. Equation (4) is thus calculated as

$$p_d(r,\theta,t) = -\frac{\beta\omega_d^2 P_1 P_2}{8\pi\rho_0 c_0^4 r}\frac{e^{jk_d r - j\omega_d t}}{\alpha_{(1,2)} + jk_d\tan^2(\theta)/2} + c.c. \tag{5}$$

$$= -\frac{\beta\omega_d^2 P_1 P_2}{4\pi\rho_0 c_0^4 r}\left|\frac{1}{\alpha_{(1,2)} + jk_d\tan^2(\theta)/2}\right|\cos(\omega t - k_d r - \phi) \tag{6}$$

$$= KP_1P_2D_W(\theta)\cos(\omega t - k_d r - \phi), \tag{7}$$

where

$$K = \frac{\beta\omega_d^2}{4\pi\alpha_{(1,2)}\rho_0 c_0^4 r}; \tag{8}$$

Westervelt's directivity is denoted as

$$D_W(\theta) = \left|\frac{\alpha_{(1,2)}}{\alpha_{(1,2)} + jk_d\tan^2(\theta)/2}\right| = \frac{\alpha_{(1,2)}}{\sqrt{\alpha_{(1,2)}^2 + k_d^2\tan^4(\theta)/4}}; \tag{9}$$

and the angular response is given by

$$\phi = \pi - \tan^{-1}\frac{k_d\tan^2(\theta)}{2\alpha_{(1,2)}}. \tag{10}$$

They are decomposed into the integration of extremely narrow beams that are independent in all directions. In each direction, Westervelt's derivation is valid. Assuming that only weak nonlinear interactions occur in the parametric loudspeaker, the wave superposition principle is still applicable for the difference-frequency wave. Thus, the directivity of the difference-frequency wave becomes a convolution between Westervelt's directivity and the product directivity $D_1(\theta)D_2(\theta)$, *i.e.*

$$D_d(\theta) = [D_1(\theta)D_2(\theta)] \otimes D_W(\theta), \tag{11}$$

where $\otimes$ denotes the linear convolution operation. The pressure level of the difference-frequency wave is readily written as

$$p_d(r,\theta,t) = KP_1P_2D_d(\theta)\cos(\omega t - k_d r - \phi). \tag{12}$$

2.1. Extending the Convolution Model by Spectral Analysis

Equation (11) is previously known as the convolution model. It provides an accurate and concise directivity model for the parametric loudspeaker when there are only two ultrasonic primary frequencies. In order to extend the convolution model to work with different modulation methods, the pressure level of the primary sound field at a distance x and time t is modified based on the spectral analysis as

$$p_i(x,t) = \sum_{n=1}^{N} P_n e^{-\alpha_n x}\cos(\omega_n t - k_n x + \psi_n), \tag{13}$$

where N denotes the number of ultrasonic primary frequencies that are transmitted in extremely narrow and perfectly collimated beams; and ψ_n denotes the initial phase.

Every two of the ultrasonic primary frequencies result in a difference-frequency wave. The same difference frequency can be produced by different combinations of

ultrasonic primary frequencies. Such combinations are collected in a set, which is defined as $W(\omega_d) = \{i, j|\omega_i - \omega_j = \omega_d\}$. The pressure level of the difference-frequency wave is superimposed as

$$p_d(r,\theta,t|\omega_d) = \sum_{i,j\in W(\omega_d)} \left[-\frac{\beta\omega_d^2 P_i P_j}{8\pi\rho_0 c_0^4 r} \frac{e^{j(k_d r - \omega_d t + \psi_i - \psi_j)}}{\alpha_{(i,j)} + jk_d \tan^2(\theta)/2} + c.c. \right] \tag{14}$$

$$= \left[K_0 \sum_{i,j\in W(\omega_d)} P_i P_j K_{(i,j)} D_{W_{(i,j)}}(\theta) \right] + c.c., \tag{15}$$

where

$$K_0 = \frac{\beta\omega_d^2}{8\pi\rho_0 c_0^4 r} e^{jk_d r - j\omega_d t}; \tag{16}$$

$$K_{(i,j)} = \frac{e^{j\phi_{(i,j)}}}{\alpha_{(i,j)}}; \tag{17}$$

$$\phi_{(i,j)} = \psi_i - \psi_j + \pi - \tan^{-1} \frac{k_d \tan^2\theta}{2\alpha_{(i,j)}}; \tag{18}$$

and Westervelt's directivity is generalized as

$$D_{W_{(i,j)}}(\theta) = \frac{\alpha_{(i,j)}}{\sqrt{\alpha_{(i,j)}^2 + k_d^2 \tan^4(\theta)/4}}. \tag{19}$$

Similarly, when beam patterns of the ultrasonic primary frequencies are introduced as $D_n(\theta)$, the pressure level and directivity of the difference-frequency wave become

$$p_d(r,\theta,t|\omega_d) = \left\{ K_0 P_1 P_2 \sum_{i,j\in W(\omega_d)} \{[D_i(\theta) D_j(\theta)] \otimes [K_{(i,j)} D_{W_{(i,j)}}(\theta)]\} \right\} + c.c. \tag{20}$$

and

$$D_d(\theta|\omega_d) = \left| \sum_{i,j\in W(\omega_d)} \{[D_i(\theta) D_j(\theta)] \otimes [K_{(i,j)} D_{W_{(i,j)}}(\theta)]\} \right|, \tag{21}$$

respectively. This results in the extended convolution model with Westervelt's directivity. Compared with (11), the complex coefficient $K_{(i,j)}$ caters to the fact that the same difference frequencies generated by different combinations of ultrasonic primary frequencies possess different phases.

The extended convolution model can be used to compute the total harmonic distortion (THD) level of the parametric loudspeaker with respect to the observation angle as

$$THD_W(\theta|\omega_d) = \frac{\sqrt{\sum_{n=2} n^4 D_d(\theta|n\omega_d)^2}}{D_d(\theta|\omega_d)} \times 100\%. \tag{22}$$

2.2. Extending the Convolution Model by Berktay's Far-field Solution

After Westervelt published his discovery of the parametric acoustic array, Berktay studied a self-demodulation phenomenon caused by the same nonlinear acoustic effect [3]. Berktay theoretically verified that when an acoustic wave was transmitted in the form of a pulsed carrier, it would self-demodulate to its envelope, which consisted of much lower frequency components than the ultrasonic carrier frequency after a sufficiently long propagation distance. Using Berktay's far-field solution is an alternative way to extend the convolution model to work with different modulation methods.

The pressure level of the primary sound field at a distance x and time t is written in an amplitude-modulated form as

$$p_i(x,t) = P_c e^{-\alpha_c x} f\left(t - \frac{x}{c_0}\right) \cos(\omega_c t - k_c x), \tag{23}$$

where P_c, α_c and ω_c are the amplitude, attenuation rate and angular frequency of the ultrasonic carrier frequency, respectively; $k = \omega/c_0$ is the wavenumber of the ultrasonic carrier frequency; and $f(t)$ is an envelope function, varying very slowly as compared to the ultrasonic carrier.

By substituting (23) into (2) and discarding the second harmonic of the ultrasonic carrier frequency, the source strength density of the secondary wave is written as

$$q_d(x,t) = \frac{\beta P_c^2}{2\rho_0^2 c_0^4} e^{-2\alpha_c x} \frac{\partial}{\partial t}\left\{ f^2\left(t - \frac{x}{c_0}\right)\right\}. \tag{24}$$

Equation (24) is rewritten in the frequency domain as

$$Q_d(x, j\omega) = \frac{\beta P_c^2}{2\rho_0^2 c_0^4} e^{-2\alpha_c x} j\omega F_0(x, j\omega) e^{-jk_d x}, \tag{25}$$

where $q_d(x,t) \leftrightarrow Q_d(x, j\omega)$ and $f^2(t) \leftrightarrow F_0(j\omega)$ are Fourier transform pairs. Moreover, the Fourier transform of (4) is written as

$$P_d(r, \theta, j\omega) = \frac{\rho_0}{4\pi} \int_0^{+\infty} \frac{j\omega e^{-jk_d R(x)}}{R(x)} Q_d(x, j\omega) dx, \tag{26}$$

where $p_d(r,\theta,t) \leftrightarrow P_d(r,\theta,j\omega)$ is a Fourier transform pair.

Using the geometry shown in figure 2, $R(x)$ can be approximated by r in the denominator and by $r - x + x\ tan^2(\theta)/2$ in the complex exponent. Substituting (25) into (26) yields the pressure level of the self-demodulated wave in the frequency domain as

$$P_d(r, \theta, j\omega) = \frac{\beta P_c^2}{8\pi\rho_0 c_0^4 r} \frac{(j\omega)^2 F_0(j\omega) e^{-jk_d r}}{2\alpha_c + jk_d \tan^2(\theta)/2}. \tag{27}$$

Letting $\theta = 0$ yields the Berktay's far-field solution, which is written as

$$p_d(r,\theta,t) = \frac{\beta P_c^2}{16\pi\alpha_c\rho_0 c_0^4 r} \frac{\partial^2}{\partial t^2}\left\{ f^2\left(t - \frac{r}{c_0}\right)\right\}. \tag{28}$$

Taking the absolute value of (27) yields

$$|P_d(r, \theta, j\omega)| = K_1 \omega^2 |F_0(j\omega)| D_B(\theta|\omega), \tag{29}$$

where

$$K_1 = \frac{\beta P_c^2}{16\pi\alpha_c\rho_0 c_0^4 r} \tag{30}$$

and

$$D_B(\theta|\omega) = \frac{\alpha_c}{\sqrt{\alpha_c^2 + k_d^2 \tan^4(\theta)/16}}. \tag{31}$$

$D_B(\theta|\omega)$ is referred to as Berktay's directivity in this paper.

Denoting the beam pattern of the ultrasonic carrier frequency as $D_c(\theta)$, the pressure level and directivity of the self-demodulated wave become

$$|P_d(r,\theta,j\omega_d)| = K_1\omega_d^2|F_0(j\omega_d)|D_c^2(\theta) \otimes D_B(\theta|\omega_d) \tag{32}$$

and

$$D_d(\theta|\omega_d) = D_c^2(\theta) \otimes D_B(\theta|\omega_d), \tag{33}$$

respectively. This results in the extended convolution model with Berktay's directivity. The directivity of the self-demodulated wave is expressed as the convolution of Berktay's directivity and the squared beam pattern of the ultrasonic carrier frequency.

In this case, the THD level of the parametric loudspeaker with respect to the observation angle is obtained as

$$THD_B(\theta|\omega_d) = \frac{\sqrt{\sum_{n=2}^{\infty} n^4|F_0(j\omega_{nd})|D_d(\theta|n\omega_d)^2}}{|F_0(j\omega_d)|D_d(\theta|\omega_d)} \times 100\%, \tag{34}$$

where $F_0(j\omega)$ is readily calculated after the modulation method is determined.

3. RESULTS

3.1. Simulation setup

The numerical simulation was carried out by using the k-wave toolbox [26, 27]. The simulation area was a $11.664m \times 10.64m$ rectangle. There was a perfect matching layer (PML) on the outermost layer of the area to minimize reflections. Transducers were placed on the left side of the simulation area. Each transducer had a width of $0.01m$ and the spacing between the centers of two neighbouring transducers were also $0.01m$. Thus, the ultrasonic emitter consisting of 8 transducers had a total width of $0.08m$. Sensors were arranged in an arc with the radius of $10m$ on the right side of the simulation area. A schematic diagram of the simulation setup is shown in figure 3(a). The measured frequency response of a real ultrasonic emitter was taken into account in the simulation by an infinite impulse response (IIR) filter. The modeled frequency response is plotted in figure 3(b). The other parameters regarding the numerical simulation are listed in table 1. Since the simulation setup was mainly consistent with the experiment setup, the simulation results are discussed together with the experiment results in Section 3.3.

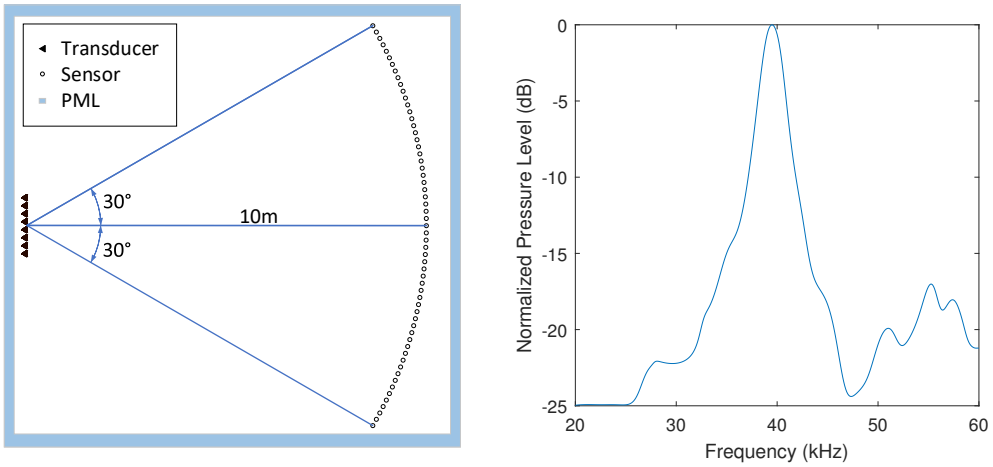

(a) Schematic diagram (b) Modeled frequency response

Figure 3. Setup of the numerical simulation in the k-wave toolbox.

Table 1. List of simulation parameters.

Parameter	value
`Number of transducer points`	8
`Number of sensor points`	5320
`Temperature`	10 °C
`Relative humidity`	50 %
`Sound speed`	343.42 m/s
`Density of air`	1.293 kg/m^3
`Power law absorption pre-factor`	1.6 $dB/(MHz)^y cm$
`Power law absorption exponent(y)`	1.984
`Number of grid points in the row direction`	5832
`Number of grid points in the column direction`	5320
`Grid point size`	0.002 m
`Thickness of PML`	0.08 m

3.2. Measurement setup

The measurement setup is illustrated in figure 4. Measurements were carried out in a room, of which the dimension was measured to be $4m \times 3m \times 3m$. The temperature was about $10°C$ and the relative humidity was in the range of $40\% - 60\%$. The interior of the measurement room was treated with sound-absorbing materials, except for the ceiling and the floor. Hence, two acoustic panels ($0.6m \times 0.6m$) were placed above and below the measurement microphone to absorb reflections from the ceiling and the floor. The acoustic panels were made up of sound absorbing materials and they were set $0.12m$ apart.

The ultrasonic emitter consisted of 8×16 piezoelectric transducers that were configured in a rectangular array. This ultrasonic emitter was fastened on a motorized rotation stage, in order for the horizontal directivities of the primary and self-demodulated waves to be measured from $-20°$ to $+20°$. Resonant frequencies and

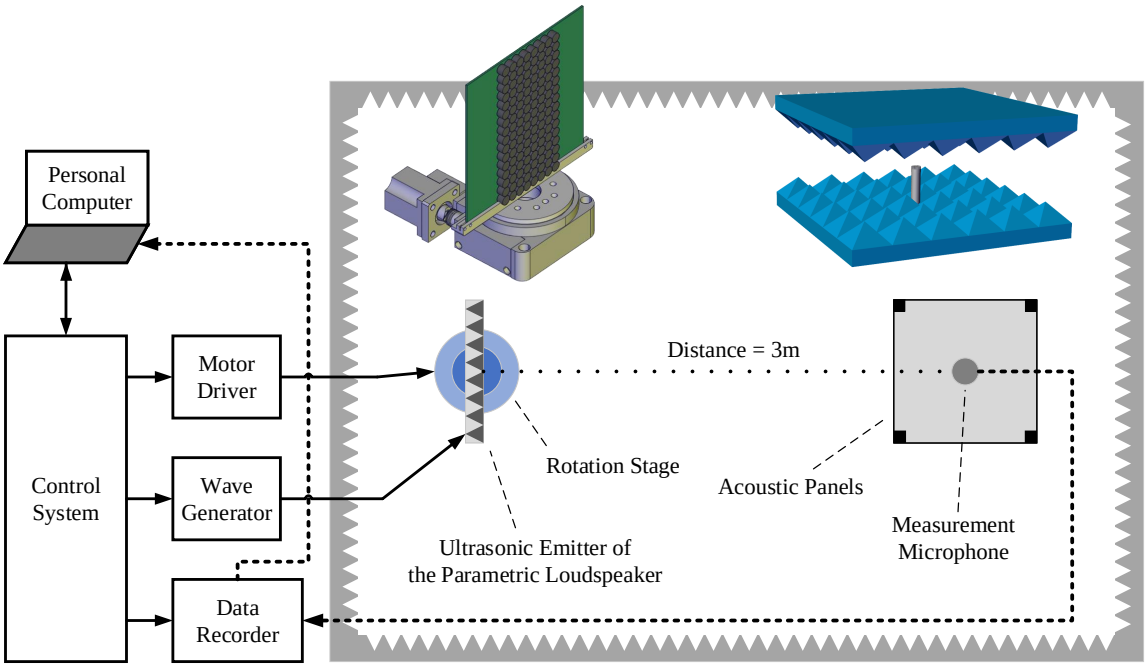

Figure 4. Measurement setup.

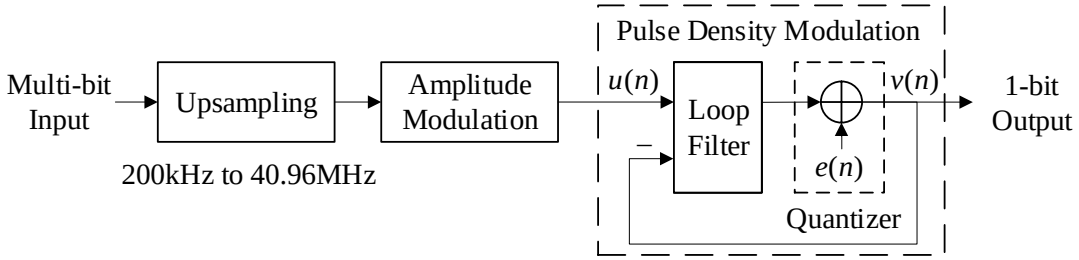

Figure 5. Block diagram of signal processing flow in the wave generator of the laboratory-made parametric loudspeaker.

diameters of the piezoelectric transducers were about $40kHz$ and $9.8mm$, respectively. The overall size of the ultrasonic emitter was $0.08m \times 0.16m$ and the Rayleigh distance was calculated as $1.49m$. The measurement microphones (CRY-333 and CRY-343) were placed at a far-field position, which was $3m$ from the ultrasonic emitter. The initial pressure level of the ultrasonic emitter was set to $110dB$, in order to satisfy the condition of applying Berktay's far-field solution. In this case, the Gol'dberg number was smaller than 1.

The laboratory-made parametric loudspeaker adopted a wave generator as the driver of the ultrasonic emitter. This wave generator converted a multi-bit audio input into a 1-bit amplitude-modulated output. The signal processing flow is shown in figure 5. The pulse density modulation (PDM) was carried out in a topology of cascade-of-

resonators feedforward form, of which the signal model is written as

$$U(z) = STF(z)V(z) + NTF(z)E(z), \tag{35}$$

where $U(z)$, $V(z)$, and $E(z)$ are the z transforms of the input $u(n)$, output $v(n)$, and quantization error $e(n)$ of the PDM. The signal transfer function (STF) and noise transfer function (NTF) were designed as

$$STF(z) = 1 \tag{36}$$

and

$$NTF(z) = \frac{(z^2 - 1.976z + 1)(z^2 - 1.958z + 1)}{(z^2 - 1.488z + 0.5672)(z^2 - 1.651z + 0.7831)}, \tag{37}$$

respectively.

3.3. Discussions

Figure 6 shows the directivities of the laboratory-made parametric loudspeaker when the audio inputs are $2kHz$ and $4kHz$ sinusoid signals. Since the DSB modulation is employed, the second harmonic is also observed besides the fundamental frequency. In figure 6(a), the average prediction errors for the fundamental frequency are 0.0577, 0.0512, and 0.0524 by the extended convolution model with Westervelt's directivity, the extended convolution model with Berktay's directivity, and the numerical simulation, respectively. The average prediction errors for the second harmonic are 0.0653, 0.0570, and 0.1277 by the extended convolution model with Westervelt's directivity, the extended convolution model with Berktay's directivity, and the numerical simulation, respectively. In figure 6(b), the average prediction errors for the fundamental frequency are 0.0477, 0.0410, and 0.0502 by the extended convolution model with Westervelt's directivity, the extended convolution model with Berktay's directivity, and the numerical simulation, respectively. The average prediction errors for the second harmonic are 0.0445, 0.0389, and 0.0500 by the extended convolution model with Westervelt's directivity, the extended convolution model with Berktay's directivity, and the numerical simulation, respectively. Those prediction errors can generally be considered small within the half-power beamwidth (HPBW), but relatively large outside the HPBW. The accuracy of the extended convolution model is overall satisfactory. It is validated that the proposed extended convolution models can predict the directivities of the parametric loudspeaker using the amplitude modulation.

The calculation of the THD beam pattern involves the division between two predicted directivities. Therefore, it is sensitive to the error in the denominator, which is given by the directivity of the fundamental frequency. The accuracy of the extended convolution model also depends on the measured directivities of the ultrasonic primary frequencies. Due to the noise floor in the measurement room, errors are incurred in the measured directivities of the ultrasonic primary frequencies at large observation angles. The extended convolution model with Berktay's directivity is simpler to calculate than the extended convolution model with Westervelt's directivity. However, the accuracy

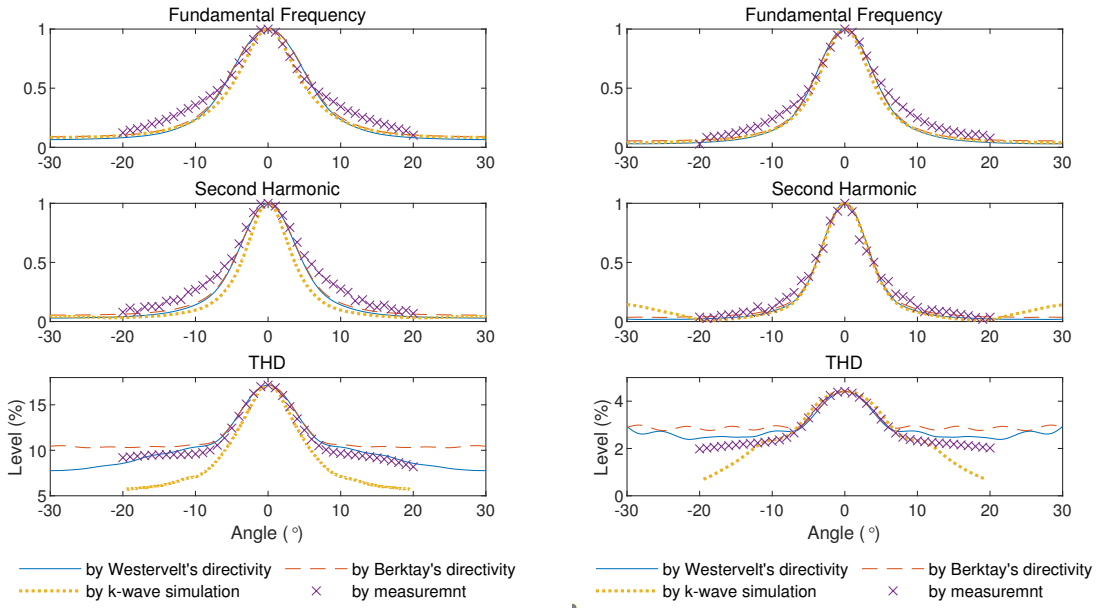

(a) $2kHz$ sinusoid audio input (b) $4kHz$ sinusoid audio input

Figure 6. Directivities of the laboratory-made parametric loudspeaker when the audio inputs are (a) $2kHz$ and (b) $4kHz$ sinusoid signals.

of the former is lower than that of the latter when the angle is more than $\pm 10°$ off the axis.

Figure 7 shows the HPBW of the laboratory-made parametric loudspeaker. The average prediction errors for the fundamental frequency are 1.8238°, 1.9484°, and 1.5030° by the extended convolution model with Westervelt's directivity, the extended convolution model with Berktay's directivity, and the numerical simulation, respectively. The average prediction errors for the second harmonic are 1.4795°, 1.4422°, and 2.8751° by the extended convolution model with Westervelt's directivity, the extended convolution model with Berktay's directivity, and the numerical simulation, respectively. Although error accumulation is difficult to eliminate, the measured HPBW shows a decreasing trend with respect to the increasing fundamental frequency as well as the second harmonic. The same trends are also predicted by the extended convolution model and the numerical simulation results.

Lastly, figure 8 demonstrates the frequency responses of the laboratory-made parametric loudspeaker both on and off the axis, since previous works on the parametric loudspeaker seldom exhibit the THD performance and frequency response off the axis. The predicted frequency responses by the extended convolution model are in good agreement with the measured frequency responses. The average prediction errors on the axis are $2.1526dB$ and $2.7287dB$ by the extended convolution model with Westervelt's directivity and the extended convolution model with Berktay's directivity, respectively. The average prediction errors off the axis are $1.4092dB$ and $1.5404dB$ by the extended convolution model with Westervelt's directivity and the extended convolution model

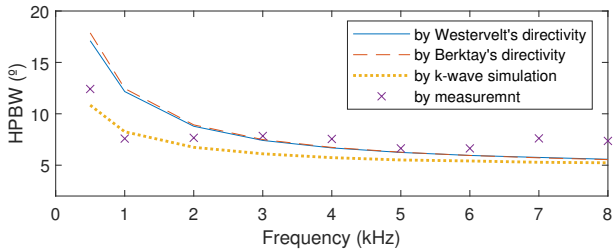

(a) Fundamental frequency

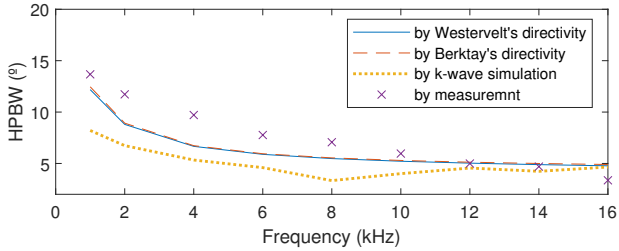

(b) Second harmonic

Figure 7. Half-power beamwidths of the laboratory-made parametric loudspeaker at the (a) fundamental frequency and the (b) second harmonic.

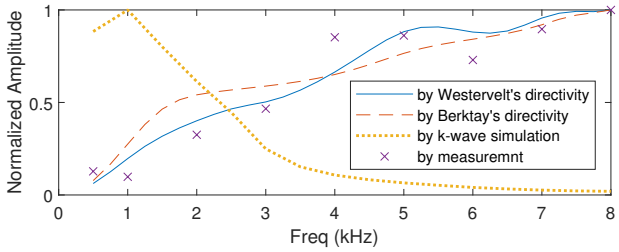

(a) On the axis

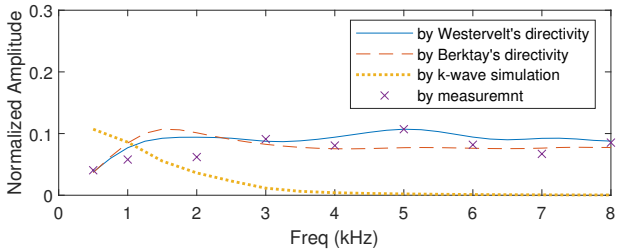

(b) Off the axis at the angle of 10°

Figure 8. Frequency responses of the laboratory-made parametric loudspeaker (a) on the axis and (b) 10° off the axis.

with Berktay's directivity, respectively. The numerical simulation encounters mistakes in calculating the frequency response. This is likely due to the windowing effect in the transformation from the time domain to the k-space, or the inaccurate computation of the sound absorption in the low-frequency range.

4. CONCLUSIONS

This paper proposes the extended convolution model with Westervelt's directivity and Berktay's directivity respectively. The extended convolution model with Westervelt's directivity treats the primary sound field as a set of ultrasonic primary frequency combinations based on the spectral analysis. Complex weighting coefficients are introduced in the wave superposition to cater to the fact that the same difference frequencies generated by different combinations of ultrasonic primary frequencies possess different phases. The extended convolution model with Berktay's directivity furthermore formulates the directivity of the self-demodulated wave as the convolution of Berktay's directivity and the squared beam pattern of the ultrasonic carrier frequency. Therefore, the extended convolution model with Berktay's directivity is simpler to calculate than the extended convolution model with Westervelt's directivity. Both of them are significantly less complicated computationally than the numerical simulation. The measurement, numerical simulation and model results are compared in terms of the directivity, THD beam pattern, and frequency response of the self-demodulated wave. It is validated that the extended convolution models provide accurate predictions to the measurement results. Thus, they can be applied in future works on the design of modulation methods for the parametric loudspeaker.

Acknowledgements

This manuscript is prepared based on the research work supported by the Civil Aviation Administration of China (Joint Grant No. U1933127) and National Natural Science Foundation of China (Grant No. 61701090). The authors would also like to thank Mr. Jing Ren and Ms. Ruyu Bai for their assistance in the course of preparing this manuscript.

[1] Westervelt P J 1960 Parametric end-fire array *Journal of the Acoustical Society of America* **32** 934-935
[2] Westervelt P J 1963 Parametric acoustic array *Journal of the Acoustical Society of America* **35** 535-537
[3] Berktay H 1965 Possible exploitation of non-linear acoustics in underwater transmitting applications *Journal of Sound and Vibration* **2** 435-461
[4] Yoneyama M, Fujimoto J, Kawamo Y and Sasabe S 1983 The audio spotlight: An application of nonlinear interaction of sound waves to a new type of loudspeaker design *Journal of the Acoustical Society of America* **73** 1532-1536
[5] Kim W and Sparrow V 2002 Audio application of the parametric array-implementation through a numerical model *Proceedings of the 113th Convention of Audio Engineering Society* 1–16
[6] Aoki K, Kamakura T and Kumamoto Y 1991 Parametric loudspeaker—characteristics of acoustic field and suitable modulation of carrier ultrasound *Electronics and Communications in Japan (Part III: Fundamental Electronic Science)* **74** 76-82
[7] Kamakura T 1984 Developments of parametric loudspeaker for practical use *Proceedings of the 10th International Symposium on Nonlinear Acoustics* 147-150
[8] Shi C and Kajikawa Y 2016 Effect of the ultrasonic emitter on the distortion performance of the parametric array loudspeaker *Applied Acoustics* **112** 108-115
[9] Kite T D, Post J T and Hamilton M F 1998 Parametric array in air: Distortion reduction by preprocessing *Proceedings of the 16th International Congress on Acoustics* **2** 1091-1092
[10] Shi C and Kajikawa Y 2016 Automatic gain control for parametric array loudspeakers *Proceedings of the 2016 IEEE International Conference on Acoustics, Speech and Signal Processing* 589-593
[11] Hatano Y, Shi C and Kajikawa Y 2017 Compensation for nonlinear distortion of the frequency modulation-based parametric array loudspeaker *IEEE/ACM Transactions on Audio, Speech, and Language Processing* **25** 1709-1717
[12] Tanaka K, Shi C and Kajikawa Y 2017 Binaural active noise control using parametric array loudspeakers *Applied Acoustics* **116** 170-176
[13] Takeoka S and Yamasaki Y 2010 Acoustic projector using directivity controllable parametric loudspeaker array *Proceedings of 20th International Congress on Acoustics* 921-925
[14] Nakadai K and Tsujino H 2005 Towards new human-humanoid communication: listening during speaking by using ultrasonic directional speaker *Proceedings of the 2005 IEEE International Conference on Robotics and Automation* 1483-1488
[15] Kimura K, Hoshuyama O, Tanikawa T and Hirose M 2011 VITA: visualization system for interaction with transmitted audio signals. *ACM SIGGRAPH 2011 Posters* 54
[16] Ueta M, Hoshuyama O, Narumi T, Tanikawa T and Hirose M 2012 JUKE cylinder: A device to metamorphose hands to a musical instrument *ACM SIGGRAPH 2012 Emerging Technologies* 13
[17] Gan W S, Tan E L and Kuo S M 2011 Audio projection: directional sound and its application in immersive communication *IEEE Signal Processing Magazine* **28(1)** 43-57
[18] Aoki K, Kamakura T and Kumamoto Y 1994 A parametric loudspeaker—applied examples *Electronics and Communications in Japan (Part III: Fundamental Electronic Science)* **77(1)** 64-74
[19] Gan W S, Yang J, Tan K S and Er M H 2006 A digital beamsteerer for difference frequency in a parametric array *IEEE Transactions on Audio, Speech, and Language Processing* **14** 1018-1025
[20] Shi C and Kajikawa Y 2015 A convolution model for computing the far-field directivity of a parametric loudspeaker array *Journal of the Acoustical Society of America* **137** 777-784
[21] Donley J 2018 Reproduction of personal sound in shared environments *PhD Thesis* University of Wollongong
[22] Arnela M, Martínez-Suquía C and Guasch O 2021 Characterization of an omnidirectional parametric loudspeaker with exponential sine sweeps *Applied Acoustics 182* 108268
[23] Guasch O and Sánchez-Martín P 2018 Far-field directivity of parametric loudspeaker arrays set

on curved surfaces *Applied Mathematical Modelling* **60** 721-738

[24] Zhong J, Kirby R and Qiu X 2021 The near field, Westervelt far field, and inverse-law far field of the audio sound generated by parametric array loudspeakers *Journal of the Acoustical Society of America* **149(3)** 1524-1535

[25] Zhong J, Kirby R, Karimi M and Zou H 2021 A cylindrical expansion of the audio sound for a steerable parametric array loudspeaker *Journal of the Acoustical Society of America* **150(5)** 3797-3806

[26] Treeby B E, Jaros J, Rendell A P and Cox B 2012 Modeling nonlinear ultrasound propagation in heterogeneous media with power law absorption using a k-space pseudospectral method *Journal of the Acoustical Society of America* **131** 4324-4336

[27] Treeby B E, Wise E S, Kuklis F, Jaros J and Cox B T 2020 Nonlinear ultrasound simulation in an axisymmetric coordinate system using a k-space pseudospectral method *Journal of the Acoustical Society of America* **148** 2288-2300